



UNIVERSITÀ DEGLI STUDI DI MILANO  
FACOLTÀ DI SCIENZE E TECNOLOGIE

Bachelor's Degree in Physics

**Next-to-Leading Order QCD Corrections to Scattering Processes Using  
 $\theta$ -Parameters in the Nested Soft-Collinear Subtraction Scheme**

Supervisor:  
Prof. Raoul Horst Röntsch

Student:  
Lucrezia Bioni  
Matr.: 13655A

Academic Year 2024–2025

# Abstract

Quantum Chromodynamics (QCD) corrections at next-to-leading order (NLO) are an essential component of high-precision theoretical predictions in high-energy particle physics. The nested soft-collinear subtraction (NSC) scheme provides an established framework for computing these corrections, offering an efficient method for handling infrared (IR) divergences through a nested factorization of soft and collinear singularities. This approach ensures proper cancellation of divergences. In this work, we focus on hadronic scattering processes and we extend the NSC framework by implementing  $\theta$ -parameters, which systematically restrict the subtraction procedure to the singular, unresolved regions of phase space. This refinement is designed to further enhance the scheme's numerical stability and computational efficiency by optimizing the treatment of IR-sensitive contributions.

# Contents

<b>1</b>	<b>Introduction</b>	<b>1</b>
1.1	The Standard Model . . . . .	1
1.2	Collider physics . . . . .	1
1.3	QCD and hard scattering processes . . . . .	2
1.4	Hadronic cross-section and factorization theorem . . . . .	2
1.5	Partonic cross-section . . . . .	5
1.6	Infrared poles and their cancellation . . . . .	7
<b>2</b>	<b>NLO QCD corrections in the NSC Subtraction Scheme</b>	<b>9</b>
2.1	Properties of Soft and Collinear partons . . . . .	9
2.2	Why a subtraction method . . . . .	10
2.3	Soft and Collinear operators . . . . .	11
2.4	Modularity of the scheme . . . . .	12
2.5	Soft limit . . . . .	13
2.6	Alternative . . . . .	15
2.7	Collinear limit . . . . .	16
2.8	Soft-collinear limit . . . . .	16
2.9	Cancellation of poles . . . . .	16
2.10	Draft . . . . .	16
<b>3</b>	<b>NLO QCD corrections with <math>\theta</math>-parameters in the NSC Subtraction Scheme</b>	<b>17</b>
3.1	Damping factors . . . . .	17
3.2	Draft . . . . .	17
	<b>Appendices</b>	<b>19</b>
<b>A</b>	<b>Useful definitions</b>	<b>21</b>
A.1	Constants . . . . .	21
A.2	Partitions at NLO . . . . .	21
	<b>Bibliography</b>	<b>23</b>

# Introduction

## §1.1 The Standard Model

As Aristotle stated, women and men began to philosophize due to wonder. From antiquity, a profound sense of astonishment towards the natural world has driven humans to investigate phenomenological reality. This drive is so profound and innate in humanity that – starting with the first philosophers, called “Pre-Socratics” or “natural philosophers” – it led them to inquire into the nature of the “archè” ( $\acute{\alpha}\rho\chi\eta$ ), the primordial principle and fundamental constituent underlying all of nature. This enduring pursuit of fundamental knowledge evolved through the centuries and, in the last one, culminated in the experimental discovery of a multitude of subatomic particles. Their proliferation was such that it prompted the noted physicist Enrico Fermi to remark: “If I could remember the names of all these particles, I’d be a botanist”. This apparent complexity, however, has been successfully resolved through the development of a robust theoretical framework that classifies these particles and describes their interactions via gauge theories: the Standard Model (SM).

The SM is formulated within the mathematical framework of Quantum Field Theory (QFT), which unifies the principles of Quantum Mechanics and Special Relativity to describe phenomena at high energies, or equivalently, subatomic scales. Its predictions have been rigorously tested and confirmed by experiments, most notably with the discovery of the Higgs boson in 2012. Despite its success, there are significant efforts to discover Physics beyond the SM. This is driven not only by the natural attempt at falsification that should be applied to every scientific theory, but also by several phenomena that the model cannot explain. These include the existence of dark matter and dark energy, the observed matter-antimatter asymmetry, and the origin of neutrino masses [13].

## §1.2 Collider physics

One of the principal methods of research in high-energy physics is collider physics [5]. Using colliders, it is possible to artificially accelerate particles and to reach extremely high center-of-mass energy. Operating at the energy frontier is crucial: higher-energy collisions enable events with greater momentum transfer and energy deposition. These events are essential because concentrating significant energy within a tiny volume allows us to excite new, heavy elementary particles from the vacuum, and study their properties. Experiments at the energy frontier are conducted at the Large Hadron Collider (LHC) at CERN: in a 27-kilometer ring,

proton beams collide at a center-of-mass energy of approximately 13.6 TeV. Although these energy scales have allowed us to study the known fundamental interactions – with the exception of gravity – in great detail, they have not been sufficient for the discovery of new particles. Since increasing the energy of the colliding particles is not feasible with existing technology, the focus of collider experiments in the next decade will shift towards higher experimental precision. This precision is crucial for refining our understanding of the Standard Model (SM), especially the properties of the Higgs boson: in fact, it is the agent of electroweak (EW) symmetry breaking, which is a fundamental component of the theory. Moreover, precision measurements serve as a powerful probe for new physics, which may reveal itself as subtle deviations from SM predictions in processes involving only known particles. However, testing the Standard Model with experimental results necessitates reliable theoretical predictions for hadron collider processes.

### §1.3 QCD and hard scattering processes

A theoretical description of hadron collisions is complicated primarily by our limited knowledge of the strong force, which binds the elementary constituents of hadrons. Strong interactions are described by Quantum Chromodynamics (QCD), a non-Abelian gauge theory based on the SU(3) symmetry group. The QCD Lagrangian is not analytically solvable, making it extremely difficult to understand proton dynamics from first principles. A way to overcome these obstacles becomes manifest when we consider how hadrons collide at high energies [17]. Typically, they undergo either elastic scattering or diffractive dissociation: in the first case, they collide but remain intact; in the second, they disintegrate into a small number of hadrons. However, on rare occasions, a more interesting phenomenon can occur: the elementary partons that compose the hadrons can interact and exchange a large amount of momentum ( $\sim 100$  GeV). This is the case in so-called “hard scattering processes,” which are central to probing the electroweak scale, the Higgs boson, and potential new physics. Their importance is directly related to a key feature of the strong force: asymptotic freedom. The essence of this property is the weakening of the colour force at short distances [5]. In this high-energy regime, the interacting partons can be approximated as being nearly free, which permits a perturbative description of the strong interaction. The strength of these interactions is governed by the coupling constant  $\alpha_S$ . Due to asymptotic freedom,  $\alpha_S$  is on the order of 0.1 at energies relevant for contemporary colliders<sup>1</sup>. This makes the strong force about ten times stronger than the electromagnetic interaction (whose coupling constant is  $\alpha \sim 1/137$ ), yet sufficiently small to allow for the application of well-defined perturbative approximation methods.

### §1.4 Hadronic cross-section and factorization theorem

A framework for describing these short-distance hard scattering processes is provided by the collinear factorization theorem [4]. Within this framework, colliding hadrons are treated as beams of partons, each carrying a certain fraction of the hadron’s total momentum. The probability of finding a parton with a specific energy fraction is encoded in the Parton Distribution Functions (PDFs). These functions are universal, meaning they are independent of the specific

---

<sup>1</sup>This value is energy-dependent;  $\alpha_S \sim 0.1$  is typical at energies around 100 GeV.

scattering process being studied. Consequently, PDFs can be measured in one set of experiments and then used to make predictions for many others [14]. The short-distance interaction of partons produces final states composed of Standard Model particles, such as leptons, gauge bosons, and additional QCD partons. The final-state partons, which are the direct products of the perturbative calculation, cannot be observed directly due to confinement<sup>2</sup>. Instead, they evolve into collimated sprays of hadrons [10]. We interpret these partons as the seeds of hadronic jets and define the resulting sprays as jets themselves. At high energies, the properties of these jets are largely determined by the perturbative dynamics of their initiating parton and are only mildly affected by non-perturbative QCD effects.

The asymptotic freedom of QCD is what enables a perturbative description of the strong interaction. However, it is crucial to recognize that the precise mechanism allowing us to decouple the motion of partons from the proton's dynamics is the separation of energy scales involved. Interactions in the Standard Model typically probe energy scales on the order of  $Q \sim 100 \text{ GeV} - 1 \text{ TeV}$ , while the characteristic energy scale of hadronic structure and confinement is significantly lower,  $\Lambda_{\text{QCD}} \sim 100 \text{ MeV}$ .

The production cross section for final states involving QCD jets and other Standard Model particles in hard hadronic collisions is thus given by

$$d\sigma = \sum_{a,b} \int_0^1 dx_1 dx_2 f_a(x_1, \mu_F) f_b(x_2, \mu_F) d\hat{\sigma}_{a,b}(x_1, x_2, \mu_F, \mu_R; \mathcal{O}) \left( 1 + \mathcal{O}\left(\frac{\Lambda_{\text{QCD}}}{Q}\right)^n \right), \quad n \geq 1 \quad (1.1)$$

where  $f_{a,b}$  are the parton distribution functions mentioned above;  $a, b \in \{g, d/\bar{d}, u/\bar{u}, s/\bar{s}, c/\bar{c}, b/\bar{b}\}$  represent the types of partons (gluons or quarks) inside the two colliding hadrons;  $x_1, x_2$  are respectively the momentum fractions carried by partons  $a$  and  $b$ ; and  $\mathcal{O}$  is an infrared-finite observable.

The non-perturbative corrections in Eq. 1.1 are suppressed by powers of the ratio  $\Lambda_{\text{QCD}}/Q$ : in this case,  $Q$  represents the hard scale of the process, typically identified as the lowest transverse momentum ( $p_T$ ) cut applied to final-state partons. For a typical cut of  $Q \sim 20 \text{ GeV}$ , this ratio is of order  $10^{-2}$ . The exact power  $n$  of this suppression is process-dependent, and not always immediately evident, though for many applications the leading power is  $n = 2$ . This implies that the theoretical uncertainty from factorizing non-perturbative physics is of order  $\mathcal{O}(10^{-4})$ . Even when the leading power is only  $n = 1$ , the non-perturbative effects would be at the percent level ( $\sim 10^{-2}$ ). This is comparable in size to the Next-to-Next-to-Leading Order (NNLO) QCD corrections for many processes. Therefore, a precise description of a process requires the inclusion of at least NNLO perturbative corrections before the inherent uncertainty from power corrections becomes significant.

This formalism establishes a clear distinction between the short-distance perturbative process and the long-distance non-perturbative physics. The boundary between these two regimes is defined by the factorization scale ( $\mu_F$ ). Processes with a momentum transfer  $Q > \mu_F$  are treated as the hard scatter of point-like partons, calculable within perturbation theory. Physics at scales  $Q < \mu_F$ , which describes how the partons are bound within the proton, is incorporated into the non-perturbative Parton Distribution Functions (PDFs).

The other scale present in the factorized cross-section in Eq. 1.1 is the renormalization scale ( $\mu_R$ ). Its necessity arises because the calculation of partonic interactions in QCD using Feyn-

---

<sup>2</sup>Quark confinement is the phenomenon that prevents quarks and gluons from propagating as free particles over macroscopic distances.

man diagrams often results in ultraviolet (UV) divergences. These infinities do not indicate a fundamental error in the theory, but suggest a distinction between the bare parameters in the Lagrangian and physically observable quantities. The process of renormalization allows us to absorb these divergences into a redefinition of the Lagrangian's parameters, providing finite expressions for measurable quantities. The consequence of this procedure is that the coupling constant becomes a function of the energy scale, a phenomenon known as “running” [5]. The renormalization scale  $\mu_R$  is the energy at which the coupling constant is defined, thereby encapsulating the quantum corrections of the theory.

Throughout this thesis, we set  $\mu_F = \mu_R = \mu$ . While a physical prediction must be independent of these arbitrary scales, cross-sections calculated within a fixed-order perturbative expansion exhibit a dependence on both the renormalization and factorization scales. Therefore, varying the scales around a central value and observing how the prediction changes provides a standard method for estimating the uncertainty associated with the truncation of the perturbative series.

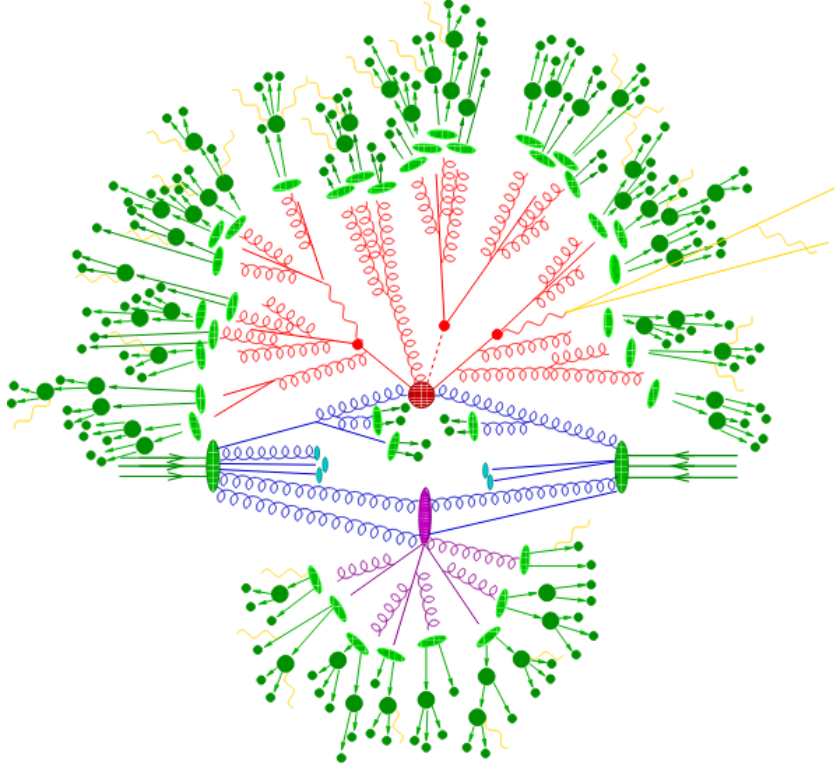


Figure 1.1: Sketch of an hard hadron-hadron collision at a collider like the LHC. The central red blob represents the hard interaction, a high-energy collision between two partons, calculable using perturbative QCD. The incoming and outgoing partons emit initial-state (blue) and final-state (red) radiation, producing many secondary particles. Softer underlying event activity (purple) arises from additional partonic interactions within the protons. A key feature is the hierarchy of energy scales: the hard process occurs at high energies ( $Q > \Lambda_{\text{QCD}}$ ), while subsequent radiation and hadronization (green) take place at progressively lower scales, eventually transitioning to non-perturbative physics around  $\Lambda_{\text{QCD}}$ . Figure from [11].

Referring to Eq. 1.1, we can state that only the left-hand side represents a physically measurable quantity. The right-hand side, in contrast, consists of unobservable components: the parton

distribution functions (PDFs), which are extracted from experimental data, and the partonic cross-section  $d\hat{\sigma}_{a,b}$ , which is calculable within perturbation theory. It is therefore essential to understand how this latter quantity is computed.

## §1.5 Partonic cross-section

We consider the inclusive<sup>3</sup> production of  $N$  jets at a hadron collider, together with a color-neutral system  $X$

$$pp \rightarrow X + N \text{ jets}. \quad (1.2)$$

As discussed above, we can use asymptotic freedom of QCD to expand the partonic cross section  $d\hat{\sigma}_{a,b}$  in Eq. 1.1 in powers of the strong and the electroweak coupling constants,  $\alpha_s$  and  $\alpha$ ,

$$d\hat{\sigma}_{a,b} = d\hat{\sigma}_{a,b}^{(0,0)} + \alpha_s d\hat{\sigma}_{a,b}^{(1,0)} + \alpha_s^2 d\hat{\sigma}_{a,b}^{(2,0)} + \alpha_s^3 d\hat{\sigma}_{a,b}^{(3,0)} + \alpha d\hat{\sigma}_{a,b}^{(0,1)} + \alpha\alpha_s d\hat{\sigma}_{a,b}^{(1,1)} + \dots \quad (1.3)$$

Due to the different values of the coupling constants, at the same order they have a different impact on the final result: at NLO, QCD corrections account for approximately 10%, while EW account for 1%; at NNLO, QCD corrections account for 1%. Throughout this thesis, we will focus on the calculation of NLO QCD corrections.

The first term in this expansion  $d\hat{\sigma}_{a,b}^{(0,0)} \equiv d\hat{\sigma}_{a,b}^{\text{LO}}$  is called Leading Order (LO), and it is defined as [20]

$$2s_{a,b} d\hat{\sigma}_{a,b}^{\text{LO}} = \mathcal{N} \int d\Phi (2\pi)^4 d\text{Lips}_X \delta^{(4)}(p_{\mathcal{H}_f} + p_X - p_a - p_b) |\mathcal{M}_0(p_a, p_b; p_{\mathcal{H}_f}, p_X)|^2 \mathcal{O}(p_{\mathcal{H}}, p_X). \quad (1.4)$$

With  $\mathcal{H}_f$ , we denote the list of final-state resolved particles, and  $p_{\mathcal{H}_f}$  is their momentum, while  $p_X$  denotes the momentum of the color-singlet in the hard process.  $\mathcal{N}$  is a normalization factor: it takes into account color and spin averages as well as symmetry factors. With  $s_{a,b}$ , we express the partonic center-of-mass energy squared:  $s = (p_a + p_b)^2 = 2p_a \cdot p_b$ , considering massless partons. The matrix element for the considered process is denoted by  $\mathcal{M}_0$ , and  $\mathcal{O}$  represents an infrared-safe observable that ensures the final state contains at least  $N$  resolved jets. This latter feature is crucial because infrared dynamics are non-perturbative and, consequently, cannot be described by an expansion in  $\alpha_s$ . Finally,  $d\text{Lips}_X$  is the Lorentz-invariant phase space for the colorless particle  $X$ , including the momentum-conserving delta function, and  $d\Phi$  is the Lorentz-invariant phase space for the final-state particles.

$$d\Phi = \prod_{i \in \mathcal{H}_f} [dp_i], \quad [dp_i] = \frac{d^3 p_i}{(2\pi)^3 2E_i}, \quad (1.5)$$

where  $[dp_i]$  is the phase-space element of a final-state parton  $i$ . Moreover, in Eq. 1.4, summation over spins and colors of final-state partons, and averaging over spins and colors of initial-state partons are assumed.

For notational compactness, we introduce the function  $F_{\text{LM}}^{ab}$ , defined as in Section 2 of [19]

$$F_{\text{LM}}^{ab} = d\text{Lips}_X |\mathcal{M}_0|^2 \mathcal{O}. \quad (1.6)$$

---

<sup>3</sup>The inclusive cross-section counts every collision event that creates a specific particle, whether it appears alone, with jets, or with any other additional radiation. It gives the total production rate, ignoring the details of what else is produced alongside it.



We denote the integration over the final-state phase space of Eq. 1.6 with the angular brackets  $\langle \dots \rangle$ , and obtain exactly Eq. 1.4

$$2s_{a,b} d\hat{\sigma}_{a,b}^{\text{LO}} = \langle F_{\text{LM}}^{ab}[\dots] \rangle. \quad (1.7)$$

At Leading Order (LO), calculations are performed directly. The tree-level matrix elements can be computed easily using helicity techniques and colour-subamplitude decompositions [3], and are then integrated, either numerically or analytically.

The strong coupling constant in hard scattering processes is small enough to allow for a perturbative description, but not enough to make higher-order corrections entirely negligible. Therefore, in order to claim high precision, we also need to compute QCD corrections. According to the factorization theorem, the computed partonic cross-section should be insensitive to long-distance effects, which are absorbed into the parton distribution functions. The QCD corrections instead account for short-distance, high-energy effects at higher orders in the coupling constant. The NLO correction  $d\hat{\sigma}_{a,b}^{(1,0)} \equiv d\hat{\sigma}_{a,b}^{\text{NLO}}$  to a partonic cross section consists of three terms: the one-loop (virtual) contribution, the real emission contribution, and the contribution related to parton distribution functions

$$d\hat{\sigma}_{a,b}^{\text{NLO}} = d\hat{\sigma}_{a,b}^{\text{V}} + d\hat{\sigma}_{a,b}^{\text{R}} + d\hat{\sigma}_{a,b}^{\text{pdf}}. \quad (1.8)$$

The last term,  $d\hat{\sigma}_{a,b}^{\text{pdf}}$ , is generated by the renormalization of the PDFs at LO, and its expression is known [7]. The other terms,  $d\hat{\sigma}_{a,b}^{\text{V}}$  and  $d\hat{\sigma}_{a,b}^{\text{R}}$ , are related to either the emission of an additional leg in the Feynman diagram, i.e., an extra parton in the final state (real correction), or to the emission and reabsorption of a parton through a loop (virtual correction).

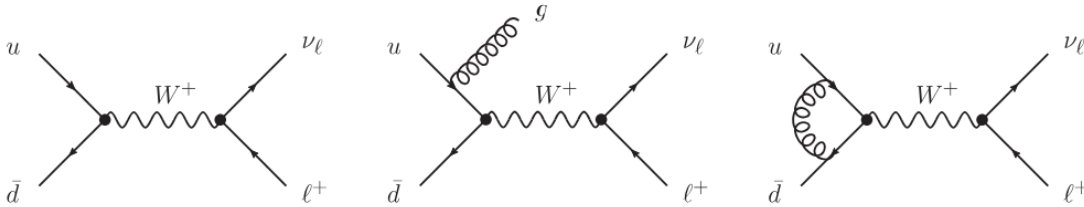


Figure 1.2: Feynman diagrams for W boson production at hadron colliders. The diagram on the left corresponds to the leading-order (LO) calculation of the total cross-section. The diagrams shown in the middle and on the right represent the real and virtual corrections, respectively, which together constitute the next-to-leading-order (NLO) contributions to the total cross-section. Figure from [13]

It is important to emphasize that while the concepts of “real” and “virtual” radiation are physically well-defined, their separate contributions to the partonic cross-section,  $d\hat{\sigma}_{a,b}$ , are not physically observable. The division into real and virtual terms is therefore a computational tool, introduced to organize the calculation and manage the various contributions more effectively. The treatment of these terms is non-trivial, as they exhibit divergences in specific energy regimes. The virtual contributions, for instance, contain ultraviolet (UV) singularities. These are removed through the process of renormalization<sup>4</sup>, a procedure that ensures physical observables, when expressed in terms of appropriately defined renormalized parameters, become

<sup>4</sup>Throughout this thesis, we work with UV-renormalized matrix elements.

insensitive to the high-energy UV region.

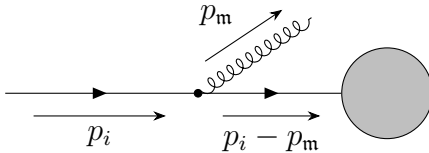
Furthermore, the low-momentum (soft) and small-angle (collinear) kinematic regions produce singularities in both the real and virtual contributions. These infrared (IR) singularities are not independent: the real and virtual corrections are fundamentally linked by their infrared behavior. The divergence of scattering amplitudes in the soft or collinear limit means these kinematic configurations must be carefully handled to obtain meaningful results. Consequently, a precise procedure for removing these divergences is of the highest importance for calculating finite cross-sections.

## §1.6 Infrared poles and their cancellation

In order to deal with IR divergences, it is convenient to employ dimensional regularization [2]. This technique involves the analytical continuation of momentum space from 4 to  $d = 4 - 2\epsilon$  dimensions, where  $\epsilon \in \mathbb{C}$  and  $\text{Re}(\epsilon) < 0$ . In this framework, divergences appear as poles in  $1/\epsilon$  in the complex dimensional plane.

The virtual corrections  $d\hat{\sigma}_{a,b}^V$  contain explicit infrared and collinear poles, which are independent of the details of the hard matrix element [7]. In contrast, the real emission contribution  $d\hat{\sigma}_{a,b}^R$  contains kinematic singularities that only become explicit  $1/\epsilon$  poles upon integration over the phase space of the additional final-state parton. However, we must avoid a naive integration over the entire radiation phase space, as it would render the cross section inclusive rather than differential, discarding all information on the kinematics of the radiated parton. This information is often crucial since jet properties provide essential data for defining experimental signatures.

QCD amplitudes for real emission processes become singular in kinematic limits where the gluon becomes soft (low energy) or any parton (quark, antiquark, gluon) is emitted collinearly to another parton. In these limits, the propagator of the emitted particle approaches its on-shell condition, leading to divergent behavior. To show this, consider a diagram that describes an emission of a gluon ( $\mathbf{m}$ ) off an external incoming quark ( $i$ ) line



$$\sim \frac{1}{(p_i - p_m)^2} = \frac{1}{2E_i E_m (1 - \cos \theta_{im})} \xrightarrow{E_m, \theta_{im} \rightarrow 0} \infty.$$

For massless partons ( $|\mathbf{p}_i| = E_i$ ,  $|\mathbf{p}_i|^2 = 0$ ), the amplitude exhibits a clear divergence in both the soft and collinear limits, that is when  $E_m$  or  $\theta_{im} \rightarrow 0$ .

It is important to consider the origin of these infinities. The presence of divergences is, in fact, a manifestation of long-distance effects: they signal that non-perturbative contributions are entering our perturbative calculation. This could be a problem, as we lack methods to treat non-perturbative QCD effects from first principles [14]. Fortunately, once the  $1/\epsilon$  poles are extracted from both the virtual and real corrections, their sum is guaranteed to be free of infrared divergences due to the Bloch-Nordsieck [1] and Kinoshita-Lee-Nauenberg theorems. Therefore, perturbative QCD corrections remain insensitive to the details of infrared physics. However, achieving the cancellation of the  $1/\epsilon$  poles by simply summing the real and virtual corrections is not straightforward. This complication arises because the virtual corrections are defined in an  $n$ -particle phase space, whereas the real corrections inhabit an  $(n + 1)$ -particle

phase space. We might think that this problem could be avoided by integrating over the phase space. However, this approach would only yield a total cross-section, not a differential one, as stated above. This mismatch in the dimensionality of the integration domains, combined with the need to extract the implicit  $1/\epsilon$  poles from the real-emission contributions, without performing the full integration, is precisely why dedicated subtraction schemes are required. Over time, various methods have been developed to perform fully differential QCD computations for hadron collider processes, both at NLO and NNLO. Among the existing methods, in this thesis we will focus on the Nested Soft-Collinear (NSC) Subtraction Scheme [12], which will be detailed in Chapter 2. The numerical stability and computational efficiency of this method can, however, be further improved. A step forward in this direction will be presented in Chapter 3; this represents the original contribution of this thesis.

# NLO QCD corrections in the NSC Subtraction Scheme

The singular limits of NLO QCD amplitudes, as well as the methods for using them to compute NLO QCD cross sections, are well established [6, 7]. Furthermore, all the singular limits of QCD amplitudes necessary for calculating NNLO QCD corrections have been known for approximately two decades. However, it took significant time to determine how to combine these NNLO limits with the ideas from the NLO Frixione-Kunszt-Signer (FKS) subtraction scheme [6] to construct a valid subtraction method for NNLO computations. Among the numerous proposed methods, the Nested Soft-Collinear Subtraction Scheme (NSC SS), introduced in [12], is particularly attractive, for reasons that will become clear throughout the following discussion.

This chapter provides an overview of the main results achieved. Since the objective of this thesis is to implement parameters that allow for greater control over the integrated phase-space region, and since these parameters appear only in the real corrections, we will focus exclusively on the latter. Moreover, the divergent parts of the virtual corrections can be isolated using Catani's representation of renormalized one-loop scattering amplitudes [8]. Although these methods have been implemented up to NNLO, this thesis will focus on the NLO case, as its relative simplicity offers a clearer understanding of how to implement the parameters.

## §2.1 Properties of Soft and Collinear partons

The desired method necessitates the isolation of singularities in the real corrections without integrating over the momenta of any of the final-state particles, in order to keep the kinematics of all the final-state particles intact. There are two key insights that allow us to overcome this obstacle. The first one is related to the behaviour of NLO QCD amplitudes at soft and collinear limits.

For a generic QCD amplitude  $\mathcal{M}$  involving  $n$  partons with four-momenta  $p_1, p_2, \dots, p_n$  and an additional soft gluon with vanishing four-momentum  $p_m$ , the squared amplitude factorizes into (i) the squared amplitude for the hard process without the gluon and (ii) an eikonal factor that depends only on the color charges and momenta of the hard partons and the momentum of the soft gluon ( $p_m$ ) [9]

$$\lim_{E_m \rightarrow 0} |\mathcal{M}(p_1, p_2, \dots, p_n; p_m)|^2 = -4\pi\alpha_s \mu^{2\epsilon} \sum_{i,j=1}^n \mathcal{S}_{ij}(p_m) \vec{T}_i \cdot \vec{T}_j |\mathcal{M}_0(p_1, p_2, \dots, p_n)|^2, \quad (2.1)$$

where the general eikonal factor is

$$\mathcal{S}_{ij}(p_{\mathbf{m}}) = \frac{p_i \cdot p_j}{(p_i \cdot p_{\mathbf{m}})(p_j \cdot p_{\mathbf{m}})}, \quad (2.2)$$

and the square of the color charges are  $\vec{T}_i^2 = C_F$  if  $i$  is a quark or an anti-quark, and  $\vec{T}_i^2 = C_A$  if  $i$  is a gluon.

Whereas, in the collinear limit, i.e., the limit where a gluon is emitted parallel to a quark, the amplitude-squared factorizes into (i) a splitting function, which describes the probability for the quark to radiate the gluon collinearly at a given energy, and (ii) the squared hard amplitude, which now depends on the resulting quark momentum after the emission

$$\lim_{\theta_{i\mathbf{m}} \rightarrow 0} |\mathcal{M}(p_1, \dots, p_n; p_{\mathbf{m}})|^2 \sim P_{f_{[i\mathbf{m}]}f_i} |\mathcal{M}_0(p_1, \dots, p_i + p_{\mathbf{m}}, \dots, p_n)|^2. \quad (2.3)$$

The unresolved parton  $\mathbf{m}$  could also be a quark or an antiquark. However, the emission of a soft quark leads to a convergent integral; consequently, no divergences are associated with soft quark or antiquark emissions. Divergences do arise in the collinear limit, but, as in the gluon case, the amplitude factorizes into a hard process involving a parton with rescaled momentum and a corresponding splitting function.

Equation 2.1 shows that the dependence on  $p_{\mathbf{m}}$  lies only in the eikonal function, while  $\mathcal{M}_0$  is independent of  $p_{\mathbf{m}}$ . Instead, Equation 2.3 shows that the dependence on the unresolved momentum is absorbed into the rescaled momentum of parton  $i$  within the hard matrix element  $\mathcal{M}_0$ , while the singular behavior is captured by the splitting function. These remarks will be fundamental to construct properly a subtraction method.

The second important insight is that, in singular kinematic regions, real emissions are always unresolved, meaning they lack a distinct experimental signature. Consequently, we can safely integrate over the singular regions of their phase space without losing any physically observable information.

## §2.2 Why a subtraction method

Let us first present the core idea of the subtraction formalism. We consider the integral

$$I = \int_0^1 dx \frac{1}{x^{1+\epsilon}} F(x), \quad (2.4)$$

where  $F(x)$  is an arbitrary function regular at  $x = 0$ . The integrand diverges at the lower limit, and this singularity is regulated by the parameter  $\epsilon$ , which ultimately produces a  $1/\epsilon$  pole upon integration. We want to isolate this pole analitically, and define the integral in such a way that the limit  $\epsilon \rightarrow 0$  can be taken safely. To achieve this, we write  $F(x) = [F(x) - F(0)] + F(0)$

$$I = \int_0^1 dx \frac{1}{x^{1+\epsilon}} [F(x) - F(0)] + F(0) \int_0^1 dx \frac{1}{x^{1+\epsilon}}, \quad (2.5)$$

and, performing the integration in the second term, we get

$$I = \int_0^1 \frac{dx}{x} [F(x) - F(0)] - \frac{1}{\epsilon} F(0) + \mathcal{O}(\epsilon). \quad (2.6)$$

This equation demonstrates that we have successfully isolated the  $1/\epsilon$  pole in  $I$  and regulated the integrand. As a result, the  $\epsilon \rightarrow 0$  limit can now be taken safely, leaving an integral that is regular at  $x = 0$  and can be evaluated numerically.

Now, suppose we have a function  $\mathcal{S}$  that reproduces the leading singular behaviour of  $F_{\text{LM}}^{ab}$  (defined in Eq. 1.6) in all soft and collinear limits, and that can be integrated in the  $d$ -dimensional phase space of the unresolved parton  $\mathbf{m}$ . We can then write the real-emission cross section as

$$2s_{a,b} d\hat{\sigma}_{a,b}^{\text{R}} = \int [dp_{\mathbf{m}}] F_{\text{LM}}^{ab} = \int [dp_{\mathbf{m}}] (F_{\text{LM}}^{ab} - \mathcal{S}) + \int [dp_{\mathbf{m}}] \mathcal{S} \quad (2.7)$$

where  $[dp_{\mathbf{m}}]$  is the  $d$ -dimensional phase-space measure for the emitted gluon, now also incorporating the theta function to enforce energy conservation

$$[dp_{\mathbf{m}}] = \frac{d^{d-1}p_{\mathbf{m}}}{(2\pi)^{d-1}2E_{\mathbf{m}}} \theta(E_{\text{max}} - E_{\mathbf{m}}), \quad (2.8)$$

and  $E_{\text{max}}$  is an arbitrary energy scale that must be at least as large as the maximum energy allowed by the momentum-conserving  $\delta$ -functions in Eq. 1.4.

On the right-hand side of Eq. 2.7, the first term is integrable in four-dimensional phase space, since the leading singular behaviour of  $F_{\text{LM}}^{ab}$  is removed by the subtraction term  $\mathcal{S}$ . As this integration is performed numerically using Monte Carlo (MC) methods, it is clear that restricting the integration region to the minimal necessary volume is crucial for improving the efficiency of the computation.

The second term involves only the unresolved parton  $\mathbf{m}$ , making it possible to integrate over its phase space without affecting the jet observables. Furthermore, as showed in Eq. 2.6, this integration enables the extraction of  $1/\epsilon$  poles, which describe the singular behaviour of  $\mathcal{S}$  and, consequently, of the amplitude itself. Moreover, it resolves the problem of the dimensional mismatch between the integration domains of the virtual and real corrections. Thus, the cancellation of the poles with those arising from the virtual contributions becomes possible.

## §2.3 Soft and Collinear operators

Different subtraction schemes are characterized by different forms for  $\mathcal{S}$ , or, equivalently,  $F(0)$ . The FKS subtraction scheme, which constitutes the basis for the NSC method, constructs  $\mathcal{S}$  directly from the soft and collinear limits. The efficacy of this approach becomes clear if we consider the behaviour of the amplitudes in these limits, as detailed in Section 2.1: in both the soft and collinear cases, the amplitude squared factorizes into a lower-multiplicity function  $F_{\text{LM}}^{ab}$ , which is independent of the unresolved parton  $\mathbf{m}$ , and a singular term, whose integration over the phase space of parton  $\mathbf{m}$  gives the explicit pole. Therefore, we introduce two operators that perform soft and collinear projections

$$S_i A = \lim_{E_i \rightarrow 0} A, \quad C_{ij} A = \lim_{\rho_{ij} \rightarrow 0} A, \quad (2.9)$$

where  $\rho_{ij} = 1 - \vec{n}_i \cdot \vec{n}_j = 1 - \cos \theta_{ij}$ , with  $\vec{n}_i$  a unit vector that describes the direction of the momentum of the  $i$ -th particle in  $(d-1)$ -dimensional space, and  $\theta_{ij}$  the angle between partons  $i$  and  $j$ . These operators apply to all terms that follow them.

Thus, we identify  $\mathcal{S}$  as the action of the soft and/or collinear operators on  $F_{\text{LM}}^{ab}$ . As these operators capture the leading asymptotic behaviour of the product of the matrix element squared,

the observable, and the phase space – namely, the definition of  $F_{\text{LM}}^{ab}$  in Eq. 1.6, if this quantity is, instead, integrable, the operator acts as an annihilator (e.g.,  $S_q = S_{\bar{q}} = 0$ ).

The singularities are isolated and extracted sequentially in a nested manner: first, the soft singularities are removed, followed by the collinear and soft-collinear ones, using an identity operator constructed as follows:

$$\mathbb{1} = S_{\mathbf{m}} + \sum_{i \in \mathcal{H}} \bar{S}_{\mathbf{m}} C_{i\mathbf{m}} + \sum_{i \in \mathcal{H}} \bar{S}_{\mathbf{m}} \bar{C}_{i\mathbf{m}} \omega^{\mathbf{m}i}, \quad (2.10)$$

where  $\bar{S}_{\mathbf{m}} = \mathbb{1} - S_{\mathbf{m}}$ ,  $\bar{C}_{\mathbf{m}} = \mathbb{1} - C_{\mathbf{m}}$ ,  $\mathcal{H} = \mathcal{H}_f \cup \{a, b\}$ , and  $\omega^{\mathbf{m}i}$  are partition functions that allow for treating one collinear singularity at a time by splitting the phase space, and satisfy the following equation

$$\sum_{i \in \mathcal{H}} \omega^{\mathbf{m}i} = 1. \quad (2.11)$$

It is also convenient to partition the phase space in such a way that some partons are classified as “hard” and thus cannot give rise to infrared singularities. For this purpose, we define so-called “damping factors” (see Appendix A.2), which can be used to construct a partition of unity

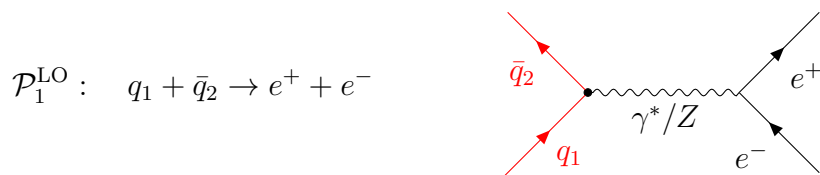
$$\sum_{i \in \mathcal{H}_f} \Delta^{(i)} = 1. \quad (2.12)$$

The damping factor  $\Delta^{(i)}$  acts as an annihilator, vanishing when any parton other than  $i$  becomes unresolved.

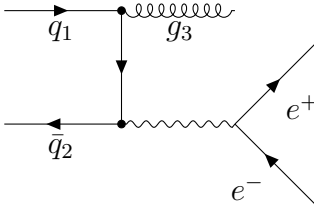
## §2.4 Modularity of the scheme

One of the most interesting features of the NSC subtraction scheme is its modular structure: the subtractions for a generic process, no matter how complicated, are built from a relatively small set of basic ingredients. Indeed, the soft contributions are straightforward to compute, while, for the nested-soft-collinear ones, we only need to consider pairs of partons. This leads to three possible cases: both partons are initial state, both are final state, or one is initial and one is final. These three possibilities have been studied in [15], [16], and [18], respectively. Therefore, in order to better understand the workings of the NSC subtraction scheme with all its subtleties, the following sections will present a general treatment, while making explicit reference to specific examples, namely the processes discussed in [15] and [16].

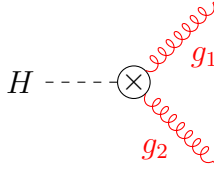
Ref. [15] provides the analytic formulas for the production of a generic color-singlet final state  $V$  at a hadron collider, i.e.,  $q_1 \bar{q}_2 \rightarrow V$  (which we will call  $\mathcal{P}_1^{\text{LO}}$ ), such as the Drell-Yan process, illustrated in the following diagram



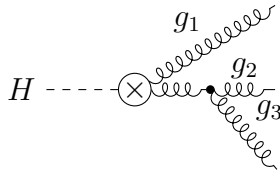
The real emission contribution refers to the process  $\mathcal{P}_1^{\text{NLO}} : q_1 \bar{q}_2 \rightarrow V + g_3$ , that, in the case of Drell-Yan, can be represented as

$$\mathcal{P}_1^{\text{NLO}} : \quad q_1 + \bar{q}_2 \rightarrow e^+ + e^- + g_3$$


Instead, Ref. [16] considers the decay of a color-singlet particle  $Q$  into quarks and gluons, and, in particular, the process  $\mathcal{P}_2^{\text{LO}} : Q \rightarrow f_i f_j + X$ , where  $\{f_i, f_j\}$  can be either  $\{g, g\}$  or  $\{q, \bar{q}\}$ . We will focus on the discussion of the decay to a  $gg$  final state since its singularity structure is more complex: once the corrections for  $Q \rightarrow gg$  are understood, the corrections for  $Q \rightarrow q\bar{q}$  are easily derived. This process, if for instance  $Q$  is the Higgs boson, is represented by the following diagram

$$\mathcal{P}_2^{\text{LO}} : H \rightarrow g_1 + g_2$$


where  $\otimes$  denotes the effective local vertex, which encapsulates the top-quark loop contribution. NLO QCD contributions come from the following process

$$\mathcal{P}_2^{\text{NLO}} : H \rightarrow g_1 + g_2 + g_3$$


Our goal is to present the explicit expression for the real-emission contributions in a form similar to that of Catani's  $I_1(\epsilon)$  function defined in Ref.[8], by introducing two operators,  $I_S$  and  $I_C(\epsilon)$ , which parametrize the poles arising from the soft and collinear limits, respectively. The corrections will then be given by the product of these functions with the leading-order kinematics, so that the sum

$$I_T(\epsilon) = I_V(\epsilon) + I_S(\epsilon) + I_C(\epsilon), \quad (2.13)$$

is finite as  $\epsilon \rightarrow 0$ , where  $I_V(\epsilon)$  is related to  $I_1(\epsilon)$ .

## §2.5 Soft limit

Let  $\mathbf{m}$  be the index that characterizes the unresolved parton. To define the expression of the last term on the right-hand side of Eq. 2.7 in the soft limit, it is necessary to integrate over the phase space of the parton  $\mathbf{m}$  in Eq. 2.1, i.e., the result of the action of the soft operator on the squared matrix element. Before performing the integration, we note that it is convenient to



express the phase-space measure  $[dp_m]$  from Eq. 2.8 in hyperspherical coordinates. For massless partons (where  $|p_m| = E_m$ ), this measure becomes

$$[dp_m] = \frac{E_m^{d-3} dE_m d\Omega_{d-1}}{2(2\pi)^{d-1}} \theta(E_{\max} - E_m), \quad (2.14)$$

where  $d\Omega_{d-1}$  is the  $(d-1)$ -dimensional solid-angle element. Using the bare QCD coupling  $g_{s,b}^2 = 4\pi\alpha_s$  and considering  $N_p$  final-state partons at NLO, we obtain

$$\langle S_m F_{\text{LM}}(\mathbf{m}) \rangle = \int dE_m E_m^{d-5} \theta(E_{\max} - E_m) \int \frac{d\Omega_{d-1}}{2(2\pi)^{d-1}} (-g_{s,b}^2) \sum_{(ij)}^{N_p} \frac{\rho_{ij}}{\rho_{im}\rho_{jm}} (\vec{T}_i \cdot \vec{T}_j) F_{\text{LM}}. \quad (2.15)$$

Recall that  $\rho_{ij} = 1 - \cos\theta_{ij}$ , so that the dot product is  $p_i \cdot p_j = E_i E_j \rho_{ij}$ . We now evaluate the integrals using dimensional regularization in  $d = 4 - 2\epsilon$  dimensions. The energy integral yields a simple pole in  $\epsilon$ :

$$\int_0^{E_{\max}} \frac{dE_m}{E_m^{1+2\epsilon}} = -\frac{1}{2\epsilon} E_{\max}^{-2\epsilon}. \quad (2.16)$$

Regarding the angular integral, we utilize a standard result, given for instance in Appendix G.2 of [18]

$$\int \frac{d\Omega_{d-1}}{2(2\pi)^{d-1}} \frac{\rho_{ij}}{\rho_{ik}\rho_{jk}} = -\frac{2^{1-2\epsilon}}{\epsilon} \left[ \frac{1}{8\pi^2} \frac{(4\pi)^\epsilon}{\Gamma(1-\epsilon)} \right] \eta_{ij}^{-\epsilon} K_{ij}, \quad (2.17)$$

with

$$K_{ij} = \left[ \frac{\Gamma^2(1-\epsilon)}{\Gamma(1-2\epsilon)} \right] \eta_{ij}^{1+\epsilon} {}_2F_1(1, 1; 1-\epsilon; 1-\eta_{ij}) \quad (2.18)$$

where  $\eta_{ij} = \rho_{ij}/2$ , and  ${}_2F_1$  denotes the Gauss hypergeometric function.

Finisco soft limit, e poi adatto esempi espliciti.

In the limit where the gluon with momentum  $p_3$  becomes soft, the amplitude of the process  $\mathcal{P}_1^{\text{NLO}}$  factorizes into

$$S_3 F_{\text{LM}}(1, 2, 3) = g_{s,b}^2 2C_F \frac{\rho_{12}}{E_3^2 \rho_{13} \rho_{23}} F_{\text{LM}}(1, 2) \quad (2.19)$$

where  $g_{s,b}$  is the bare QCD coupling,  $C_F = \frac{4}{3}$  is the QCD color factor (see Eq. A.1), and  $F_{\text{LM}}(\dots)$  denotes the corresponding parton-level matrix element squared, as defined in Eq. 1.6, with the arguments specifying the partons involved in the process. The integration of this term over the phase space of the unresolved gluon gives

$$\langle S_3 F_{\text{LM}}(1, 2, 3) \rangle = \frac{2C_F[\alpha_s] \mu^{2\epsilon}}{\epsilon^2} \frac{\Gamma(1-\epsilon)^2}{\Gamma(1-2\epsilon)} (2E_{\max})^{-2\epsilon} F_{\text{LM}}(1, 2), \quad (2.20)$$

where we have introduced the short-hand notation

$$[\alpha_s] = \frac{\alpha_s(\mu)}{2\pi} \frac{e^{\epsilon\gamma_E}}{\Gamma(1-\epsilon)}, \quad (2.21)$$

with  $\alpha_s(\mu)$  the running coupling constant, and  $\gamma_E$  the Euler-Mascheroni constant.

For the process  $\mathcal{P}_2^{\text{NLO}}$ , it is convenient to partition the phase space so that some partons are identified as “hard” and cannot generate infrared singularities. To achieve this, we use the

scalar product of the gluons' four-momenta  $s_{ij} = 2p_i \cdot p_j$  and energy-momentum conservation (considering massless partons)

$$p_H^2 = (p_1 + p_2 + p_3)^2 \implies m_H^2 = s_{12} + s_{13} + s_{23}, \quad (2.22)$$

and we write the amplitude as

$$F_{\text{LM}}(1, 2, 3) = \tilde{s}_{12}F_{\text{LM}}(1, 2, 3) + \tilde{s}_{13}F_{\text{LM}}(1, 2, 3) + \tilde{s}_{23}F_{\text{LM}}(1, 2, 3) = 3\tilde{s}_{12}F_{\text{LM}}(1, 2, 3), \quad (2.23)$$

where  $\tilde{s}_{ij} = s_{ij}/m_H^2$ , and we have used the symmetry of the matrix element and the phase space. The prefactor  $\tilde{s}_{12}$  ensures that gluons  $g_1$  and  $g_2$  are resolved, and that only gluon  $g_3$  can become unresolved. The soft limit of the amplitude is

$$S_3F_{\text{LM}}(1, 2, 3) = g_{s,b}^2 2C_A \frac{p_1 \cdot p_2}{(p_1 \cdot p_3)(p_2 \cdot p_3)} F_{\text{LM}}(1, 2), \quad (2.24)$$

where  $C_A = 3$  is the  $SU(3)$  color factor (see Eq. A.1). Integrating over the phase space of the gluon  $g_3$ , we get

$$\langle S_3F_{\text{LM}}(1, 2, 3) \rangle = \frac{1}{3} \frac{2C_A[\alpha_2]}{\epsilon^2} \left( \frac{m_H^2}{\mu^2} \right)^{-\epsilon} \eta_{12}^{-\epsilon} [1 + \epsilon^2(\text{Li}_2(1 - \eta_{12}) - \zeta_2) + \mathcal{O}(\epsilon^2)] F_{\text{LM}}(1, 2), \quad (2.25)$$

where  $\eta_{ij} = \rho_{ij}/2$ .

In the case of the  $\mathcal{P}_3^{\text{NLO}}$  process, in the soft limit the amplitude becomes

$$S_5F_{\text{LM}}(1, 4, 5) = g_{s,b}^2 2C_F \frac{\rho_{14}}{E_5^2 \rho_{51} \rho_{54}} F_{\text{LM}}(1, 4), \quad (2.26)$$

and, since it no longer depends on the momentum of the unresolved gluon  $g_5$ , we can integrate over its phase space

$$\langle S_5F_{\text{LM}}(1, 4, 5) \rangle = \frac{2C_F[\alpha_s]}{\epsilon^2} \left( \frac{4E_{\text{max}}^2}{\mu^2} \right)^{-\epsilon} \eta_{14}^{-\epsilon} K_{14} F_{\text{LM}}(1, 4), \quad (2.27)$$

where

$$K_{ij} = \left[ \frac{\Gamma^2(1 - \epsilon)}{\Gamma(1 - 2\epsilon)} \right] \eta_{ij}^{1+\epsilon} {}_2F_1(1, 1, 1 - \epsilon, 1 - \eta_{ij}). \quad (2.28)$$

## §2.6 Alternative

paper 2310, paragrafo 3, pag 5.

Operator  $I_S$

$$I_S(\epsilon) = -\frac{(2E_{\text{max}}/\mu)^{-2\epsilon}}{\epsilon^2} \sum_{(ij)}^{N_p} \eta_{(ij)}^{-\epsilon} K_{ij}(\vec{T}_i \cdot \vec{T}_j) \quad (2.29)$$

Operator  $I_C$

$$I_C(\epsilon) = \sum_{i=1}^{N_p} \frac{\Gamma_{i,f_i}}{\epsilon} \quad (2.30)$$

## §2.7 Collinear limit

Discorso generale su come ottengo operatore  $I_C$  nell'initial state e nel final state, e in generale che forma hanno le correzioni in questo caso.

Spiego che, siccome collinear limit è locale, piuttosto che focalizzarmi su un processo specifico, mostro cosa succede quando le varie tipologie di partoni diventano collineari: in base alla situazione, entrerà nel processo hard un partone diverso, e questo fa sì che si hanno diverse splitting functions.

## §2.8 Soft-collinear limit

## §2.9 Cancellation of poles

## §2.10 Draft

# NLO QCD corrections with $\theta$ -parameters in the NSC Subtraction Scheme

Il lavoro esposto nel capitolo precedente può essere ulteriormente generalizzato, come è stato fatto nei paper [19, 21]. In questo capitolo ripercorriamo tali risultati, implementando theta parameters. Lo facciamo perché uno dei principali difetti di NSC SS è che la sua efficienza è un po' impattata dalla numerical integration of the subtraction terms.

## §3.1 Damping factors

Quando ho tanti partoni nel final state, introduco damping factor per identificare quello unresolved. Vedere 2310, pagine 6-8.

## §3.2 Draft

Soft limit

$$\langle S_m^{\theta_s} F_{\text{LM}}(\mathbf{m}) \rangle = \int [dp_m] \theta(E_m < \theta_s E_{\text{max}}) (-g_{s,b}^2) \sum_{(ij)}^{N_p} \frac{p_i \cdot p_j}{(p_i \cdot p_m)(p_j \cdot p_m)} (\vec{T}_i \cdot \vec{T}_j) F_{\text{LM}} \quad (3.1)$$

$$\langle S_m^{\theta_s} F_{\text{LM}}(\mathbf{m}) \rangle = -[\alpha_s] \frac{(2E_{\text{max}}/\mu)^{-2\epsilon}}{\epsilon^2} \theta_s^{-2\epsilon} \sum_{(ij)}^{N_p} \langle \eta_{(ij)}^{-\epsilon} K_{ij}(\vec{T}_i \cdot \vec{T}_j) \cdot F_{\text{LM}} \rangle \quad (3.2)$$

$$\begin{aligned} &= \frac{1}{\epsilon^2} \sum_{i=1}^{N_p} T_i^2 + \frac{1}{\epsilon} \left[ - \sum_{i=1}^{N_p} 2 \log \left( \frac{2E_{\text{max}} \theta_s}{\mu} \right) \vec{T}_i^2 - \sum_{i \neq j}^{N_p} f_1(\eta_{ij}) (\vec{T}_i \cdot \vec{T}_j) \right] + \\ &+ \sum_{i=1}^{N_p} 2 \log^2 \left( \frac{2E_{\text{max}} \theta_s}{\mu} \right) \vec{T}_i^2 - \sum_{i \neq j}^{N_p} \left[ f_2(2E_{\text{max}} \theta_s) f_1(\eta_{ij}) + K_{ij}^{(2)} \right] (\vec{T}_i \cdot \vec{T}_j) + \mathcal{O}(\epsilon) \end{aligned} \quad (3.3)$$

Coefficient

$$\begin{aligned}
c_{-1}(\theta_s) &= - \sum_{i=1}^{N_p} 2 \log \left( \frac{2E_{\max} \theta_s}{\mu} \right) \vec{T}_i^2 - \sum_{i \neq j}^{N_p} f_1(\eta_{ij}) (\vec{T}_i \cdot \vec{T}_j) = \\
&= - \sum_{i=1}^{N_p} \left( 2\text{Li}^{\theta_s} + 2 \log \left( \frac{2E_i}{\mu} \right) \right) \vec{T}_i^2 - \sum_{i \neq j}^{N_p} f_1(\eta_{ij}) (\vec{T}_i \cdot \vec{T}_j)
\end{aligned} \tag{3.4}$$

Final state

Collinear limit

$$\langle C_{im}^{\theta_i} \Delta^{\mathbf{m}} F_{\text{LM}}(\mathbf{m}) \rangle = \int \dots \int [dp_i] \int [dp_{\mathbf{m}}] \frac{g_{s,b}^2}{p_i \cdot p_{\mathbf{m}}} z P_{gg}(z) F_{\text{LM}}(i\mathbf{m}) \tag{3.5}$$

$$\langle C_{im}^{\theta_i} \Delta^{\mathbf{m}} F_{\text{LM}}(\mathbf{m}) \rangle = [\alpha_s] [d\eta_{i\mathbf{m}\theta_i}] \int \dots \int [dp_i] \left( \frac{2E_i}{\mu} \right)^{-2\epsilon} \int_0^1 dz z^{1-2\epsilon} (1-z)^{-2\epsilon} P_{gg}(z) F_{\text{LM}} \tag{3.6}$$

$$\begin{aligned}
\langle C_{im}^{\theta_i} \bar{S}_{\mathbf{m}}^{\theta_s} \Delta^{\mathbf{m}} F_{\text{LM}}(\mathbf{m}) \rangle &= [\alpha_s] \left\langle \left\{ \frac{1}{\epsilon} (\gamma_g + 2\vec{T}_g^2 \text{Li}^{\theta_s}) - 2 \log \frac{2E_i}{\mu} \gamma_g + \right. \right. \\
&\quad \left. \left. - 4 \log \frac{2E_i}{\mu} \vec{T}_g^2 \text{Li}^{\theta_s} - \log \theta_i \gamma_g - 2\vec{T}_g^2 \text{Li}^{\theta_s} \log \theta_i \right\} F_{\text{LM}} \right\rangle
\end{aligned} \tag{3.7}$$

# **Appendices**



## Appendix A

---

# Useful definitions

## §A.1 Constants

We report in this section useful constants that are used throughout the thesis. We denote the color-charge operators by  $\vec{T}_i$ , whose square gives the Casimir operator of the corresponding representation of  $SU(3)$ , and identifies the color charge of the represented parton. If  $N_c$  is the number of colors, we have

$$\vec{T}_q^2 = \vec{T}_{\bar{q}}^2 = C_F = \frac{N_c^2 - 1}{2N_c}, \quad \vec{T}_g^2 = C_A = N_c. \quad (\text{A.1})$$

The expressions for quark and gluons anomalous dimensions are

$$\gamma_q = \frac{3}{2}C_F \quad \gamma_g = \frac{11}{6}C_A - \frac{2}{3}T_R n_f, \quad (\text{A.2})$$

where  $T_R = 1/2$ , and  $n_f$  is the number of massless quarks flavors. Moreover, we introduce the following shorthand

$$[\alpha_s] = \frac{\alpha_s(\mu)}{2\pi} \frac{e^{\epsilon\gamma_E}}{\Gamma(1-\epsilon)}, \quad (\text{A.3})$$

with  $\alpha_s(\mu)$  the running coupling constant, and  $\gamma_E$  the Euler-Mascheroni constant.

## §A.2 Partitions at NLO

To manage the calculation of QCD corrections for processes with many final-state particles, we introduce partitions that separate resolved and potentially unresolved partons. Following the construction proposed in [19], we consider a process with  $N_p$  partons at leading order and an arbitrary colorless final state

$$f_1(p_1) + f_2(p_2) \rightarrow f_3(p_3) + \cdots + f_{N_p}(p_{N_p}) + X. \quad (\text{A.4})$$

At NLO, we add an extra parton to the final state, in order to describe the real-emission process. The list of the  $N = N_p - 2$  final-state partons becomes  $\mathcal{H}_f = \{f_3, f_4, \dots, f_{N_p}, f_{N_p+1}\}$ . If parton  $i$  becomes unresolved, we denote the set of  $N + 1$  final-state partons as  $\mathcal{H}_f^{(i)}$ , where  $\mathcal{H}_f^{(i)} = \mathcal{H}_f / \{i\}$ , and we introduce the function

$$d^{(i)} = \prod_{k \in \mathcal{H}_f^{(i)}} p_{k,\perp} \prod_{l < m \in \mathcal{H}_f^{(i)}} (1 - \cos \theta_{lm}), \quad (\text{A.5})$$



where  $p_{k,\perp}$  is the transverse momentum of parton  $k$ .

Using the functions in Eq. A.5, we can construct the partitions

$$\Delta^{(i)} = \frac{d^{(i)}}{\sum_{i \in \mathcal{H}_f} d^{(i)}} , \quad (\text{A.6})$$

where  $i \in \mathcal{H}_f$ . Starting from their definition, it is straightforward to demonstrate that the partition functions form a partition of unity

$$\sum_{i \in \mathcal{H}_f} \Delta^{(i)} = 1 . \quad (\text{A.7})$$

If we act with the soft operator  $S_k$  on the function  $\Delta^{(i)}$ , we get

$$S_k \Delta^{(i)} = \delta_{ki} . \quad (\text{A.8})$$

Instead, if we act with the collinear operator  $C_{lm}$ , i.e., when partons  $l$  and  $m$  become collinear, we get

$$C_{lm} \Delta^{(i)} = \begin{cases} 0, & l, m \neq i, \\ 1, & l = i, m \in 1, 2, \\ z_{i,m}, & l = i, m \in \mathcal{H}_f^{(i)}, \end{cases} \quad (\text{A.9})$$

with  $z_{i,m} = \frac{E_m}{E_i + E_m}$ , and partons 1 and 2 in the initial state.

## Bibliography

- [1] F. Bloch and A. Nordsieck. “Note on the Radiation Field of the Electron”. *Phys. Rev.* **52** (1937), pp. 54–59. DOI: [10.1103/PhysRev.52.54](https://doi.org/10.1103/PhysRev.52.54).
- [2] G. 't Hooft. “Dimensional regularization and the renormalization group”. *Nuclear Physics B* **61** (1973), pp. 455–468. ISSN: 0550-3213. DOI: [https://doi.org/10.1016/0550-3213\(73\)90376-3](https://doi.org/10.1016/0550-3213(73)90376-3).
- [3] Guido Altarelli and G. Parisi. “Asymptotic Freedom in Parton Language”. *Nucl. Phys. B* **126** (1977), pp. 298–318. DOI: [10.1016/0550-3213\(77\)90384-4](https://doi.org/10.1016/0550-3213(77)90384-4).
- [4] John C. Collins and Davison E. Soper. “The Theorems of Perturbative QCD”. *Ann. Rev. Nucl. Part. Sci.* **37** (1987), pp. 383–409. DOI: [10.1146/annurev.ns.37.120187.002123](https://doi.org/10.1146/annurev.ns.37.120187.002123).
- [5] R. K. Ellis et al. *QCD and Collider Physics*. **8**. Cambridge Monographs on Particle Physics, Nuclear Physics and Cosmology. Cambridge: Cambridge University Press, 1996, p. 435. DOI: [10.1017/CB09780511628788](https://doi.org/10.1017/CB09780511628788).
- [6] S. Frixione, Z. Kunszt, and A. Signer. “Three jet cross-sections to next-to-leading order”. *Nucl. Phys. B* **467** (1996), pp. 399–442. DOI: [10.1016/0550-3213\(96\)00110-1](https://doi.org/10.1016/0550-3213(96)00110-1). arXiv: [hep-ph/9512328](https://arxiv.org/abs/hep-ph/9512328).
- [7] S. Catani and M. H. Seymour. “A General algorithm for calculating jet cross-sections in NLO QCD”. *Nucl. Phys. B* **485** (1997). [Erratum: *Nucl. Phys. B* 510, 503–504 (1998)], pp. 291–419. DOI: [10.1016/S0550-3213\(96\)00589-5](https://doi.org/10.1016/S0550-3213(96)00589-5). arXiv: [hep-ph/9605323](https://arxiv.org/abs/hep-ph/9605323).
- [8] Stefano Catani. “The Singular behavior of QCD amplitudes at two loop order”. *Phys. Lett. B* **427** (1998), pp. 161–171. DOI: [10.1016/S0370-2693\(98\)00332-3](https://doi.org/10.1016/S0370-2693(98)00332-3). arXiv: [hep-ph/9802439](https://arxiv.org/abs/hep-ph/9802439).
- [9] Stefano Catani and Massimiliano Grazzini. “Infrared factorization of tree level QCD amplitudes at the next-to-next-to-leading order and beyond”. *Nucl. Phys. B* **570** (2000), pp. 287–325. DOI: [10.1016/S0550-3213\(99\)00778-6](https://doi.org/10.1016/S0550-3213(99)00778-6). arXiv: [hep-ph/9908523](https://arxiv.org/abs/hep-ph/9908523).
- [10] Gavin P. Salam. “Towards Jetography”. *Eur. Phys. J. C* **67** (2010), pp. 637–686. DOI: [10.1140/epjc/s10052-010-1314-6](https://doi.org/10.1140/epjc/s10052-010-1314-6). arXiv: [0906.1833](https://arxiv.org/abs/0906.1833) [[hep-ph](https://arxiv.org/abs/hep-ph)].
- [11] Stefan Höche. “Introduction to parton-shower event generators”. arXiv preprint [arXiv:1411.4085](https://arxiv.org/abs/1411.4085) (2014). Lectures presented at TASI 2014. 40 pages, 12 figures. URL: <https://arxiv.org/abs/1411.4085>.
- [12] Fabrizio Caola, Kirill Melnikov, and Raoul Röntsch. “Nested soft-collinear subtractions in NNLO QCD computations”. *Eur. Phys. J. C* **77.4** (2017), p. 248. DOI: [10.1140/epjc/s10052-017-4774-0](https://doi.org/10.1140/epjc/s10052-017-4774-0). arXiv: [1702.01352](https://arxiv.org/abs/1702.01352) [[hep-ph](https://arxiv.org/abs/hep-ph)].

- [13] John Campbell, Joey Huston, and Frank Krauss. *The Black Book of Quantum Chromodynamics : a Primer for the LHC Era*. Oxford University Press, 2018. DOI: [10.1093/oso/9780199652747.001.0001](https://doi.org/10.1093/oso/9780199652747.001.0001).
- [14] K. Melnikov. “Lectures on QCD for hadron colliders”. *Proceedings of the 2017 European School of High-Energy Physics, Evora, Portugal, 6–19 September 2017*. Ed. by M. Mulders and G. Zanderighi. Vol. 3/2018. CERN Yellow Reports: School Proceedings. CERN-2018-006-SP. Geneva: CERN, 2018. DOI: [10.23730/CYRSP-2018-003.37](https://doi.org/10.23730/CYRSP-2018-003.37).
- [15] Fabrizio Caola, Kirill Melnikov, and Raoul Röntsch. “Analytic results for color-singlet production at NNLO QCD with the nested soft-collinear subtraction scheme”. *Eur. Phys. J. C* **79**.5 (2019), p. 386. DOI: [10.1140/epjc/s10052-019-6880-7](https://doi.org/10.1140/epjc/s10052-019-6880-7). arXiv: [1902.02081](https://arxiv.org/abs/1902.02081) [hep-ph].
- [16] Fabrizio Caola, Kirill Melnikov, and Raoul Röntsch. “Analytic results for decays of color singlets to  $gg$  and  $q\bar{q}$  final states at NNLO QCD with the nested soft-collinear subtraction scheme”. *Eur. Phys. J. C* **79**.12 (2019), p. 1013. DOI: [10.1140/epjc/s10052-019-7505-x](https://doi.org/10.1140/epjc/s10052-019-7505-x). arXiv: [1907.05398](https://arxiv.org/abs/1907.05398) [hep-ph].
- [17] K. Asteriadis. “Application of the nested soft-collinear subtraction scheme to the description of deep inelastic scattering”. PhD Thesis. Karlsruhe Institute of Technology (KIT), Institute for Experimental Particle Physics (EKP), 24, 2020, p. 216. DOI: [10.5445/IR/1000135340](https://doi.org/10.5445/IR/1000135340).
- [18] Konstantin Asteriadis et al. “Analytic results for deep-inelastic scattering at NNLO QCD with the nested soft-collinear subtraction scheme”. *Eur. Phys. J. C* **80**.1 (2020), p. 8. DOI: [10.1140/epjc/s10052-019-7567-9](https://doi.org/10.1140/epjc/s10052-019-7567-9). arXiv: [1910.13761](https://arxiv.org/abs/1910.13761) [hep-ph].
- [19] Federica Devoto et al. “A fresh look at the nested soft-collinear subtraction scheme: NNLO QCD corrections to N-gluon final states in  $q\bar{q}$  annihilation”. *JHEP* **02** (2024), p. 016. DOI: [10.1007/JHEP02\(2024\)016](https://doi.org/10.1007/JHEP02(2024)016). arXiv: [2310.17598](https://arxiv.org/abs/2310.17598) [hep-ph].
- [20] Federica Devoto et al. “Integrated subtraction terms and finite remainders for arbitrary processes with massless partons at colliders in the nested soft-collinear subtraction scheme” (2025). arXiv: [2509.08594](https://arxiv.org/abs/2509.08594) [hep-ph].
- [21] Federica Devoto et al. “Towards a general subtraction formula for NNLO QCD corrections to processes at hadron colliders: final states with quarks and gluons”. *JHEP* **08** (2025), p. 122. DOI: [10.1007/JHEP08\(2025\)122](https://doi.org/10.1007/JHEP08(2025)122). arXiv: [2503.15251](https://arxiv.org/abs/2503.15251) [hep-ph].